Versão do arquivo anexado / Version of attached file:

Versão do Editor / Published Version

Mais informações no site da editora / Further information on publisher's website:

https://www.scielo.br/scielo.php?script=sci_arttext&pid=S1516-14392017000800580

DOI: 10.1590/1980-5373-mr-2017-0732

Direitos autorais / Publisher's copyright statement:

Metallic Glass Formation Upon Rapid Solidification of $Fe_{60}Cr_8Nb_8B_{24}$ (at%) Alloy through LASER Cladding and Remelting

Marcos Fernandes de Carvalho[a]*, Rudimar Riva[b], João Batista Fogagnolo[c], Cláudio Shyinti Kiminami[a],

Conrado Ramos Moreira Afonso[a]

[a]*Departamento de Engenharia de Materiais - DEMa, Universidade Federal de São Carlos - UFSCar, CP 676, Rodovia Washington Luís, s/n, Jardim Guanabara, CEP 13565-905, São Carlos, SP, Brazil.*
[b]*Instituto de Estudos Avançados - IEAv, Trevo Coronel Aviador José Alberto Albano do Amarante, n°1, Putim, São José dos Campos, SP, Brazil.*
[c]*Faculdade de Engenharia Mecânica - FEM, Universidade Estadual de Campinas - UNICAMP, Rua Mendeleyev, 200, CEP 13083-860, Campinas, SP, Brazil.*

$Fe_{60}Cr_8Nb_8B_{24}$ (at%) amorphous powder and ingot were submitted to LASER cladding and remelting process, respectively. Fe-based coatings were produced using different LASER processing parameters and characterized by scanning electron microscopy (SEM), X-ray diffraction (XRD) and Vickers microhardness. All coatings obtained by LASER cladding (LC) and layers obtained by LASER surface remelting (LSR) with shorter and median interaction times (scanning speeds of 16.7 and 66.7mm/s), irrespective of overlap value, presented peaks of the crystalline phases α-Fe, Fe_2B and the FeNbB intermetallic. In addition, layers obtained by LSR with shorter interaction time (150mm/s), in general, presented only peaks of the α-Fe and Fe_2B phases, except that produced with overlap value of 20%, more amorphous. SEM results showed that, regardless of LASER process, the coatings presented cracks, some pores and FeNbB intermetallic phase. All coatings obtained by LC and that obtained with shorter interaction time, by LSR, showed a Vickers microhardness, 1086 to 1329HV and 2161 to 2294HV, respectively, significantly higher than the substrates, AISI steel: 170HV and Fe-Cr-Nb-B: 1921HV.

Keywords: *Fe-based bulk metallic glass, LASER cladding, LASER remelting, nanocrystalline phase, amorphous phase*

1. Introduction

LASER surface treatment consists of an advanced surface modification technique, in a controlled manner[1-4] and envolving high cooling rates of about 10^4 K/s[5], for production of metallurgically well-bonded coatings. Surface treatments through LASER can enhance wear and corrosion resistance of materials[6], being used in steels, reducing the progress of wear and extending tool life. An advantage of surface treatment is that carbon steels can be hardened without presenting problems of distortion and cracks and this process includes a wide variety of techniques and improves wear resistance without changing the inner part of the material. The LASER process present, also, advantage such as reduction in operational costs[7]. In addition, using LASER process is possible to obtained microstructural refinement and also to form metastable and amorphous phases.

The $Fe_{60}Cr_8Nb_8B_{24}$ (at%) bulk metallic glass (BMG) alloy presents good glass forming ability (GFA)[8,9] leading to a formation of an amorphous or nanocrystalline structure with lower critical cooling rates of the order of 10^4 K/s[5]. Due to an excellent combination of properties and low

costs, Fe-based metallic glasses have been widely studied for industrial applications. Studies using BMG alloys are of great interest due to their improved mechanical, physical and chemical properties compared to crystalline materials[10-16].

The production of metallic glass coatings by LASER cladding (LC) involves the epitaxial growth process induced by the crystalline grain's orientation of substrate[6], the high scanning speed needed in order to obtain higher cooling rates to avoid crystallization and low ductility of metallic glasses[17], which is challenging in order to produce 100% glassy coatings by LASER. Some authors obtained coatings by LASER surface remelting (LSR) and LC[2-4,6,12,18-20]. The control of the LASER parameters combination: LASER power, scanning speed and overlapping, is the key point to be studied, in order to produce coatings free of defects, which can potentially be used for different industries applications.

Based on the information background, the aim of this study is to produce coatings of $Fe_{60}Cr_8Nb_8B_{24}$ (at%) glass-former alloy on to AISI 1020 mild steel substrate by LASER cladding of pre-placed glassy atomized powders and by LASER surface remelting of its thick crystalline ingot. The microstructure, phase's formation and Vickers microhardness

*e-mail: marcosf_c@yahoo.com.br

Metallic Glass Formation Upon Rapid Solidification of Fe$_{60}$Cr$_8$Nb$_8$B$_{24}$ (at%) Alloy through LASER Cladding and Remelting

581

of the coatings surface (LC continuous tracks) and continuous layers by LSR were investigated.

2. Experimental Procedure

The Fe$_{60}$Cr$_8$Nb$_8$B$_{24}$ (at%) alloy used in this work was spray formed following a similar procedure found in the literature[21-24] in an induction melting furnace using as raw materials a ferritic stainless steel (FSS) AISI 430 with high 13% Cr content, combined with additions of Fe-67%Nb and Fe-14%B (wt%) alloys. The nominal composition was finally adjusted by adding electrolytic Fe (99.5%) and pure Nb (99.9%) elements. This alloy was processed by spray forming process, using nitrogen (N$_2$) as the atomization gas. Ingots of Fe$_{60}$Cr$_8$Nb$_8$B$_{24}$ (at%) alloy were prepared by induction melting of 80 g pieces in an arc-furnace through homogenization of pure elements Fe, Nb, Cr metals and B crystal. The total alloy charge, weighing about 1 kg, was melted in an induction furnace on the top of the atomization chamber. A superheat of 250 K over the melting temperature (1423 K) was used to homogenize the alloy prior to pouring. The molten alloy was poured into a nozzle bore of 6 mm diameter at the bottom of a tundish and then atomized by nitrogen (N$_2$) gas with a pressure of 1 MPa. The gas-to-metal ratio, ratio between the gas (G) mass flow rate (8 kg/s) and the metal (M) mass flow rate (8 kg/s), used was G/M = 1. The overspray powder was collected from the bottom of the atomization chamber and was sieved and separated into several granulometric size ranges. For this study, the atomized overspray powder with a size range < 45 μm was selected.

LASER cladding (LC) process was carried out by the pre-placed powder method, using the Fe$_{60}$Cr$_8$Nb$_8$B$_{24}$ (at%) spray formed powder with grain size < 45 μm, in order to produce coatings (continuous tracks) on to rectangular substrates (100 × 100 × 6 mm^3) of AISI 1020 mild steel. The LC coatings were prepared by placing a 0.2 mm (200 μm) thick layer of powder on the steel substrate. These layers were clad with the LASER beam under following processing parameters, LASER power of 200 W and scanning speed of 10 mm/s, LASER beam diameter of 0.5 mm at a constant focal length (distance between the LASER beam and material surface - mm), resulting in a low energy density (ED) of 40 J/mm^2 (calculated by equation 1), and varied distances between centers of the tracks, 150, 220 and 350 μm, which correspond to overlappings of 66%, 53% and 44%, respectively. LC experiments were conducted with an Yb Fiber LASER (up to 500 W) IGP in a high-purity argon gas (Ar$_{(g)}$) atmosphere (inside a glove box). Other important parameter is the interaction time, t (ms) of the LASER beam along a linear distance (mm), which is calculated by equation 2.

The ED calculations were carried out using equation (1).

$$ED = \frac{LASER\ Power}{Scanning\ speed \times Beam\ diameter} \quad (1)$$

$$t = \frac{2w}{v_d} \quad (2)$$

Where, w: LASER beam radius (mm) and v_d: LASER scanning speed (mm/s).

On the other hand, in order to produce continuous layers on to surface of Fe$_{60}$Cr$_8$Nb$_8$B$_{24}$ (at%) substrate (ingot), the LASER surface remelting (LSR) process was carried out. In these cases, the coatings were clad with the LASER power beam under different processing parameters, LASER powers of 400 W and 800 W and scanning speeds of 16.7, 66.7 and 150 mm/s (different interaction times between the LASER beam and material), focal length constant (mm), resulting, also, in low ED values, and several overlapping values (Table 1). LSR experiments were conducted with an Yb Fiber LASER (up to 2 kW - IGP Mod. YLR200), on air, only with an argon gas (Ar$_{(g)}$) flux over to sample.

The aim was to select the LASER processing parameters that allowed the production of coatings with higher volume fraction of the amorphous phase and minimum dilution in the substrates, while still creating a metallurgical bonding with the same, and good surface quality, which will be characterized in terms of its microstructure, phase composition and microhardness.

The microstructure of the coatings was analyzed using scanning electron microscopy (SEM) with a FEI Inspect S50 and Philips XL30 FEG. The phases formed in the coatings were analyzed by X-ray diffraction (XRD) using a Siemens D5005 diffractometer and Cu-K$_\alpha$ radiation. The analysis was conducted in a flat area of the continuous coating obtained by the overlapping of linear LASER tracks and at the cross-section of clad tracks by metallography technique. The microhardness of the coatings (LC) and layers (LSR) were measured with a HMV-2000 SHIMADZU microhardness tester and a Vickers pyramid-shaped diamond indenter, performed using 50 g load (HV$_{0.050}$), irrespective of LASER processing.

3. Results and Discussion

In previous works of our research group, the Fe$_{60}$Cr$_8$Nb$_8$B$_{24}$ (at%) spray-formed alloy powder and single tracks produced by LASER cladding (LC), on to AISI 1020 mild steel substrate, were characterized by X-ray diffraction (XRD) and scanning electron microscopy (SEM) techniques, using different LASER powers (200, 300 and 400 W) and scanning speeds of 10 mm/s. The most promising results (higher volume fraction of the amorphous phase) were obtained with LASER power of 200 W and scanning speed of 10 mm/s, which are described below.

XRD analysis of the powder presented a typical amorphous halo, around 2θ = 45°, which corresponds to a fully glassy powder, indicating the high glass forming ability (GFA) of this alloy (Fig. not shown). The XRD results were confirmed

by SEM analysis, where the micrographs of the powder presented particles with a smooth surface, typical of an amorphous structure, with a homogeneous composition and, also, absence of crystalline phase contrast (Fig. not shown). The $Fe_{60}Cr_8Nb_8B_{24}$ (at%) single tracks characterization, produced by LC process with several processing parameters, showed that in order to reach a glassy state (more amorphous), with a small dilution and good surface quality, was applied a small energy density (ED = 40J/mm^2) value. These small ED value were obtained as result of the adequate combination between LASER power and scanning speeds (interaction times).
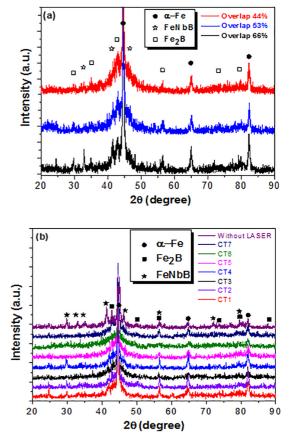
That way, in this work, the coatings produced by LC and the layers produced by LASER surface remelting (LSR) processes and characterized by different techniques, were obtained using the processing parameters mentioned previously (Experimental Procedure and Table 1).

3.1. Characterization of $Fe_{60}Cr_8Nb_8B_{24}$ (at%) coatings

3.1.1. X-ray diffraction

XRD patterns of the $Fe_{60}Cr_8Nb_8B_{24}$ (at%) coatings produced by LC and layers produced by LSR processes are presented in the Figs. 1(a)-(b), respectively. The coatings obtained by LC, on to AISI 1020 steel substrate, were produced with the same processing parameters, varying only the overlapping of 66%, 53% and 44%. The layers obtained by LSR from $Fe_{60}Cr_8Nb_8B_{24}$ (at%) substrate were produced using the processing parameters showed in the Table 1.

It can be observed in the Figure 1(a) that the $Fe_{60}Cr_8Nb_8B_{24}$ (at%) coatings produced by LC, in high-purity argon gas atmosphere, irrespective of overlap value, presented a broad peak around 2θ = 45°, indicating that it is possible to maintain, partially, the amorphous structure presents in the precursor powder, even after the superficial treatment by LASER. In addition, the diffractograms showed the sharp Bragg peaks of the crystalline phases α-Fe, Fe$_2$B and the FeNbB intermetallic[8,25], suggesting that the phase formation in the coatings was dependent of LASER power and interaction time and not of overlap value.

Figure 1. X-ray diffraction patters of $Fe_{60}Cr_8Nb_8B_{24}$ (at%) coatings produced by (a) LC with LASER power of 200 W and scanning speed of 10 mm/s at different overlaps: 66%, 53% and 44%, and layers produced by (b) LSR with LASER powers of 400 W and 800 W and scanning speeds of 16.7, 66.7 and 150 mm/s, at different overlaps: 0%, 20% 50%, 60% and 80%.

Thus, the XRD results obtained from coatings produced by LC are characteristic of a nanocrystalline structure of the primary α-Fe phase embedded in the remaining amorphous matrix. Figure 1(a) showed, also, that although the overlap value does not interfere in the formation of crystalline phases, by decreasing its value from 66% to 44% the formation of a greater fraction

Table 1. LASER processing parameters, overlaps, calculated energy density (ED, equation 1) and interaction time (equation 2), for remelted layers (CT), used in the LASER surface treatment of Fe60Cr8Nb8B24 (at%) alloy.

Remelted layers	LASER Power (W)	Scanning speed, v_d(mm/s)	Overlap (%)	ED (J/mm^2)	Interaction time, t (ms)
CT1	400	16.7	60	24	60.0
CT2	400	16.7	0	24	60.0
CT3	400	66.7	50	6	15.0
CT4	800	66.7	60	12	15.0
CT5	800	150	60	5.3	6.7
CT6	800	150	20	5.3	6.7
CT7	800	150	80	5.3	6.7

Metallic Glass Formation Upon Rapid Solidification of $Fe_{60}Cr_8Nb_8B_{24}$ (at%) Alloy through LASER Cladding and Remelting

583

of amorphous phase was favored, since less peaks of crystalline phases and a peak enlargement around $2\theta = 45°$ were observed.

Figure 1(b) showed that the $Fe_{60}Cr_8Nb_8B_{24}$ (at%) substrate (ingot), without LASER application, presented the same Bragg peaks of the crystalline phases observed in the LC process, i.e., α-Fe, Fe_2B and the FeNbB intermetallic[8,25]. In addition, the XRD patterns did not showed an amorphous halo or broad peak, indicating that the same was totally crystalline.

After the LSR process, the $Fe_{60}Cr_8Nb_8B_{24}$ (at%) layers produced with different combination of LASER parameters, presented greater fraction of glassy phase than the substrate (ingot) without LASER remelting. However, for the same LASER power, 400 W or 800 W, the fraction of glassy phase decreased for the layers produced with lower scanning speed, confirming that higher interaction times (60.0 and 15.0 ms for LASER power of 400 W and 800 W, respectively) is unfavorable to formation of glassy phase. In addition, the XRD analysis for LSR layers in Fig. 1(b) showed that, regardless of processing parameters, the layers presented a broad peak around $2\theta = 45°$, which is typical of amorphous structure, due to high glass forming ability (GFA) of $Fe_{60}Cr_8Nb_8B_{24}$ (at%) alloy and high cooling rate imposed during LSR.

It can be observed in the Fig. 1(b) that the XRD patterns of the layers produced by LSR, increasing interaction times, i.e., 15.0 to 60.0 ms (for LASER power of 400 W) and 6.6 to 15.0 s (for LASER power of 800 W), same Bragg peaks of crystalline phases than observed previously, i.e., α-Fe, Fe_2B and the FeNbB intermetallic[8,25], irrespective of overlapping (%). However, decreasing interaction times, 15.0 ms (for LASER power of 400 W) and 6.7 s (for LASER power of 800 W) according to Table 1, the LSR layers present only peaks of crystalline phases: α-Fe and Fe_2B[8], depending on overlap value. In the cases described, the crystallization of FeNbB intermetallic was inhibited at shorter interaction times, due to higher cooling rate applied, maintaining a remaining glassy phase.

Comparing the layers obtained with shorter interaction time (6.7 ms) and LASER power of 800 W, it can be noted that, decreasing the overlapping from 80% to 20%, the LSR layer presented crystalline peaks related only to primary α-Fe phase[8], indicating greater fraction of glassy phase. Similar results were observed for the LC coatings, i.e., decreasing the overlapping for the same LASER power, lead to shorter interaction time, favoring the formation of glassy phase.

For LSR process, in opposition to the LC process, the phase's formed in the layers depend on the overlapping fraction. Koga et al.[8] also observed that the $Fe_{60}Cr_8Nb_8B_{24}$ (at%) coatings produced by spray forming and powder flame spraying process - LVOF (low velocity oxygen fuel), presented peaks of the of primary α-Fe and FeNbB and Fe_2B crystalline phases.
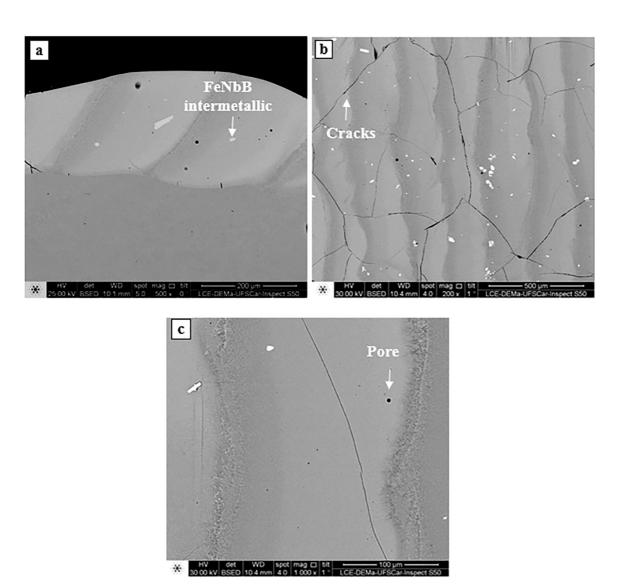
It can be concluded that, regardless of LASER process, LC or LSR , in order to obtain $Fe_{60}Cr_8Nb_8B_{24}$ (at%) coatings and layers with a higher volume fraction of the amorphous phase, the decrease in the overlap value was favorable (for the same LASER power). In the LSR process, the lower overlap value combined with shorter interaction time (for the same LASER power), also increased the volume fraction of the amorphous phase. It must be stressed that the atmosphere where the coatings and layers were produced, vacuum or air, did not interfere in the results obtained. In addition, after the LC process, the $Fe_{60}Cr_8Nb_8B_{24}$ (at%) amorphous powder had its increased crystallinity, maintaining an amorphous matrix remaining due to high GFA of this alloy. After the LSR process, the $Fe_{60}Cr_8Nb_8B_{24}$ (at%) crystalline ingot showed higher fraction of glassy phase due to higher cooling rate applied during the surface treatment.

For both case, LC and LSR, it was possible to produce coatings and layers with big volume fraction of the amorphous phase controlling the deposition parameters. According to the literature, the cooling rates that the coatings are submitted through LASER cladding can vary from 5×10^2 up to 10^4 depending on LASER parameters[26]. In this work, the cooling rate can vary significantly from LC coatings to LSR layers, even considering similar combination of LASER parameters, that would happen due to influence of substrate thickness that was 6 mm for mild steel in LC coating and around 100 mm thick for $Fe_{60}Cr_8Nb_8B_{24}$ (at%) crystalline ingot used in LSR process. Due to this fact, the heat extraction for LSR layers can lead to higher cooling rates than mentioned previously reaching greater fraction of glassy phase, according to XRD patterns (Fig. 1).

3.1.2. Scanning electron microscopy

SEM analysis in backscattered electrons (BSE) signal was realized for coating's surface and cross-section of the $Fe_{60}Cr_8Nb_8B_{24}$ (at%) LC coatings over AISI 1020 mild steel substrate, using different overlap values. Figures 2(a)-(c) present typical micrographs of the coating's microstructure produced by LC process. The coatings cross-section analysis showed a good metallurgical bond between the coating/ substrate interface, and, also, not exhibiting discontinuities, irrespective of overlap value (Fig. 2(a)). In addition, lower dilution of the coating material in the steel substrate could be observed, which is desired, leading to a lower content of the Fe from steel mixed with the coating's material composition, affecting minimally the characteristics of the $Fe_{60}Cr_8Nb_8B_{24}$ (at%) alloy powder.

Figures 2(a)-(c) showed that the coatings produced by LC, regardless of overlap value, presented cracks, some pores and FeNbB nanocrystalline intermetallic phase (light phase - higher atomic number), across the surface, and low porosity. It must be stressed that the cracks observed were formed by the entire coating surface (Fig. 2(b)), but were not very deep, since in the cross-section image (Fig. 2(a)) they were not observed. In addition, the coatings obtained from $Fe_{60}Cr_8Nb_8B_{24}$ (at%) alloy, on to AISI 1020 steel substrate, showed homogeneous distribution (without

Figure 2. Typical SEM-BSE micrographs of the (a) coating cross-section, (b) coating surface and (c) magnification of (b), produced by LC process from Fe$_{60}$Cr$_8$Nb$_8$B$_{24}$ (at%) alloy in the pre-placed spray formed powder at LASER power of 200 W and scanning speed of 10 mm/s, with different overlaps of 66%, 53% and 44%.

contrast microstructure), which suggests a low-crystallinity state, regardless of overlap value. Furthermore, it can be observed that as the overlap value decreased from 66% to 53%, the coating showed a larger area with homogeneous microstructure (smooth), which indicates higher amorphization of coating, corroborating with the XRD results (Fig. 1(a)). In addition, by decreasing the overlap value from 53% to 44% not significant change was observed, suggesting that there was an overlap limit value in which the amorphization rate maximum was achieved to LC process for this alloy.

SEM-BSE analysis of the Fe$_{60}$Cr$_8$Nb$_8$B$_{24}$ (at%) layers surface without LASER application (ingot) and layers produced by LSR, also was realized and its images are shown in the Figs. 3(a)-(f). It can be observed that the micrographs of the layer surface, without LASER application, Figs. 3(a)-(b),

showed a microstructure totally crystalline (with contrast microstructure), presenting cracks across the surface and some pores. In addition, even after the LSR process, regardless of processing parameters and overlap value, (Figs. 3(c)-(f)), the microstructure of the layers presented cracks and some pores, indicating that the cracks did not arise as a result of the LASER process.

After surface treatment by LSR, Figs. 3(c)-(f), it can be observed that the microstructure of the layers presented areas more fine, smooth and homogeneous, where the LASER beam was applied, indicating that with the LASER application, part of the substrate presented a glassy phase due to its high GFA and higher cooling rate of this process. In addition, as the interaction time decreased (15.0 to 6.7 ms) and overlap value decreased from 80% (Figs. 3(c)-(d)) to 20% (Figs.
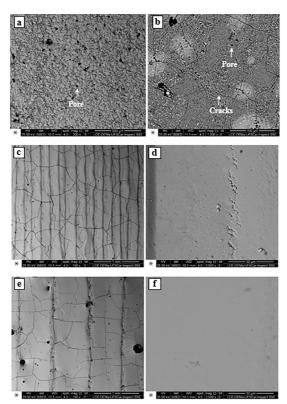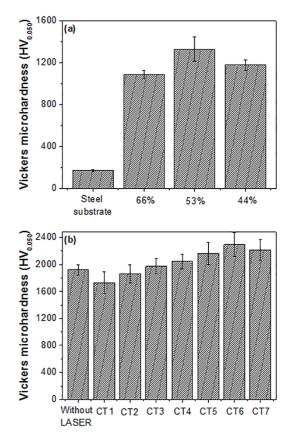
Figure 3. Typical SEM-BSE micrographs of the Fe$_{60}$Cr$_8$Nb$_8$B$_{24}$ (at%) layers surface, (a)-(b) spray formed deposit, without LASER application, and after LSR process at LASER power of 800 W and scanning speed of 150 mm/s with (low interaction time - 6.7. ms) with different overlaps: (c)-(d) 80% and (e)-(f) 20%, respectively.

Figure 4. Average Vickers microhardness of the Fe$_{60}$Cr$_8$Nb$_8$B$_{24}$ (at%) coatings surface produced by (a) LC with different overlaps, 66%, 53% and 44%, and layers by (b) LSR without LASER application and after LSR process with several processing parameters and overlap values shown in the Table 1.

3(e)-(f)), the layers showed a larger area with homogeneous microstructure (smooth), which indicates higher amorphization of the layer. Furthermore, these results were in agreement to XRD results (Fig. 1(b)) where the diffractograms showed a broad peak around the main peak, α-Fe phase (2θ = 45°), characteristic of an amorphous structure.

It can be concluded that high interaction times (low scanning speed) were not favorable to the formation of glassy phase, regardless of LSR processing parameters. Therefore, the best condition to obtain layers of Fe$_{60}$Cr$_8$Nb$_8$B$_{24}$ (at%) alloy with higher volume fraction of the amorphous phase by LSR was the combination of shorter interaction time and smaller overlaps, irrespective of LASER power. For LC process, applying the same interaction time, the optimum overlap value to obtain coatings with higher fraction of amorphous phase was smaller than or equal to 53%. It must be stressed that the atmosphere where the coatings and layers were produced, vacuum or air, did not interfere significantly in its microstructures.

3.1.3. Microhardness measurements

As mentioned previously, the Fe$_{60}$Cr$_8$Nb$_8$B$_{24}$ (at%) coatings were produced by LC with different overlaps, 66%, 53% and 44%, Fig. 4(a). Vickers microhardness measurements for these coatings showed that the average microhardness values were larger than 1086 ± 38 HV. Moreover, regardless of overlap value, the average microhardness values were much larger than AISI 1020 mild steel substrate (around 170 ± 10 HV).

It can be observed that the average microhardness value reached a maximum value of 1329 ± 118 HV for the overlap of 53%, while for the overlaps of 66% and 44% the standard deviation was lower, i.e., 1086 ± 38 HV and 1176 ± 40 HV, respectively. These results showed that there was a significant increase in the average microhardness value by decreasing the overlap value from 66% to 53%. However, the decrease of the overlap value from 53% to 44% not presented significant change in the average microhardness values, according to standard deviation. In addition, the analysis showed that the overlay of the steel substrate with Fe$_{60}$Cr$_8$Nb$_8$B$_{24}$ (at%) coatings increased the average microhardness about 8 times (≈ 782%). Although the microstructure and the phase composition of the coatings did not vary significantly with the different overlap values, they greatly influenced the Vickers microhardness values, probably due to increase of the fraction of amorphous phase as the overlap value decreased.

It should be mentioned that the greater the volume fraction of the amorphous phase formed, generally, the harder the coatings[6]. Therefore, according to results obtained from the XRD and SEM analyzes, the coatings produced by LC with overlap lower than 66%, showed a higher volume fraction of the amorphous phase and, consequently, higher average Vickers microhardness, corroborating the literature[6].

Vickers microhardness measurements of the superficial area of $Fe_{60}Cr_8Nb_8B_{24}$ (at%) layers produced by LSR are depicted in the Fig. 4(b). This Fig. showed that the average microhardness values of the $Fe_{60}Cr_8Nb_8B_{24}$ (at%) substrate, without LASER application, was 1921 ± 91 HV. After the LSR process, it can be observed that, generally, the average microhardness values increased in relation to the substrate, except to layers produced with longer interaction times, 60.0 ms, (CT1 and CT2) at LASER power of 400 W. Moreover, according to standard deviation, the average microhardness values of the layers produced with longer interaction times (scanning speed less than 150 mm/s), regardless of LASER power and overlap values, did not show significant changes in its average microhardness values.

However, by decreasing the interaction time, regardless of LASER power and overlap values, the layers produced showed greater average microhardness values. Although the microhardness value resulted higher for the overlapping of 20% (2294 ± 175 HV), when compared with the others: 80% (2161 ± 168 HV) and 60% (2215 ± 159 HV), according to standard deviation, did not show significant changes. As mentioned previous, according to SEM and XRD analyzes, it was observed higher volume fraction of the amorphous phase for the layers produced with shorter interaction time (higher cooling rate). Although there was a significant change in microstructure and phase composition of the layers by varying the processing parameters and the overlapping, did not increase, significantly, the fraction of glassy phase. The maximum microhardness value around 2300 HV for LSR Fe-Cr-Nb-B alloy opens perspectives for new technological applications, such as machining tool material. Comparing microhardness value with other hard tool materials, WC (1850 HV), Al_2O_3 (2062 HV), TiC (2425 HV) and SiC (2435 HV), it is possible to consider that the value for FeCrNbB (2300 HV) is almost equivalent to TiC and SiC (≈6% variation), and significantly greater than alumina and WC, showing outstanding microhardness for a metallic material for coating's applications.

It can be concluded from the results obtained above that for the coatings produced by LC there was an overlap limit value, 53%, where the average microhardness value was greater. On contrary, for the layers produced by LSR, the change in the overlap value did no influence the average microhardness values (for a same LASER power and interaction time). In addition, the decrease of the interaction time favored the increase in the average microhardness values of the coatings e layers.

4. Conclusions

It was concluded that by adjusting the processing parameters, LASER power, scanning speed and overlap, it was possible to obtain $Fe_{60}Cr_8Nb_8B_{24}$ (at%) coatings and layers with the desired characteristics, by LASER cladding (LC) and LASER surface remelting (LSR).

Coatings produced by LC showed that the phase composition and microstructure not varied significantly with the overlap value change. That way, the coatings presented a remaining amorphous matrix (amorphous broad peak), due to high GFA of this alloy, and nanocrystalline phases of α-Fe, Fe_2B and intermetallic FeNbB.

Microstructure was composed by FeNbB nanocrystalline intermetallic phase and low porosity, as observed by the SEM analysis. Although the microstructure of the coatings did not vary significantly with the different overlap values, they showed higher Vickers microhardness than AISI 1020 mild steel substrate (≈782%). In addition, by decreasing the overlap value from 66% to 53% there was a significant increase in the average microhardness value, i.e., from 1086 ± 38 HV to 1329 ± 118 HV, due to increased volume fraction of glassy phase in the LC.

The LSR of the $Fe_{60}Cr_8Nb_8B_{24}$ (at%) crystalline ingot produced layers with high fraction of glassy phase, due to high GFA of this alloy and higher cooling rate imposed. Characterization showed typical glassy broad peak, regardless of LASER parameters, and nanocrystalline α-Fe, Fe_2B and FeNbB intermetallic phases, depending on processing parameters.

Layers obtained with shorter interaction time (6.7 ms) and lower overlap (20%) showed higher fraction of amorphous phase, presenting only α-Fe nanocrystalline phase. LSR layers obtained with shorter interaction time showed impressive Vickers microhardness values, varying from 2161 ± 168 HV to 2294 ± 175 HV, for overlapping of 80% and 20%, respectively, much higher than that of crystalline substrate (1921 ± 91 HV).

Finally, this study confirms the potential use of LASER cladding and surface remelting processes, with controlled processing parameters, opening great perspectives of obtaining coatings and layers with higher fraction of glassy phase and greater Vickers microhardness, improving properties of substrate, for application as hard coatings in several engineering fields.

5. Acknowledgments

CBMM (Companhia Brasileira de Metalurgia e Mineração) for the donation of Fe-Nb master alloy for preparation of the FeCrNbB BMG of this work.

6. References

1. Steen WM. *Laser Material Processing*. 2nd ed. London: Springer-Velag; 1998.

2. Vilar R. Laser Alloying and Laser Cladding. *Materials Science Forum*. 1999;301:229-252.

3. Gargarella P, Almeida A, Vilar R, Afonso CRM, Rios CT, Bolfarini C, et al. Microstructural characterization of a laser remelted coating of $Al_{91}Fe_4Cr_3Ti_2$ quasicrystalline alloy. *Scripta Materialia*. 2009;61(7):709-712.

4. Jung HY, Choi SJ, Prashanth KG, Stoica M, Scudino S, Yi S, et al. Fabrication of Fe-based bulk metallic glass by selective laser melting: A parameter study. *Materials & Design*. 2015;86:703-708.

5. Aghasibeig M, Fredriksson H. Laser cladding of a featureless iron-based alloy. *Surface and Coatings Technology*. 2012;209:32-37.

6. Gargarella P, Almeida A, Vilar R, Afonso CRM, Peripolli S, Rios CT, et al. Formation of Fe-based glassy matrix composite coatings by laser processing. *Surface and Coatings Technology*. 2014;240:336-343.

7. Maier C, Schaaf P, Gonser U. Calculation of the temperature profile for laser treatment metallic samples. *Materials Science and Engineering: A*. 1992;150(2):271-280.

8. Koga GY, Nogueira RP, Roche V, Yavari AR, Melle AK, Gallego J, et al. Corrosion properties of Fe-Cr-Nb-B amorphous alloys and coatings. *Surface and Coatings Technology*. 2014;254:238-243.

9. Cheney J, Vecchio K. Development of quaternary Fe-based bulk metallic glasses. *Materials Science and Engineering: A*. 2008;492(1-2):230-235.

10. Wang HW, Dong C, Shek CH. Bulk metallic glasses. *Materials Science and Engineering: R: Reports*. 2004;44(2-3):45-89.

11. Afonso CRM. *Conformação por spray de ligas amorfizáveis a base de ferro com característica de magnetos moles*. [Thesis] São Carlos: Universidade Federal de São Carlos; 2004.

12. Balla VK, Bandyopadhyay A. Laser processing of Fe-based bulk amorphous alloy. *Surface and Coatings Technology*. 2010;205(7):2661-2667.

13. Greer AL. Metallic glasses...on the threshold. *Materials Today*. 2009;12(1-2):14-22.

14. Chen SH, Chan KC, Wu FF, Xia L. Achieving high energy absorption capacity in cellular bulk metallic glasses. *Scientific Reports*. 2015;5:10302.

15. Chen SH, Chan KC, Yue TM, Wu FF. Highly stretchable kirigami metallic glass structures with ultra-small strain energy loss. *Scripta Materialia*. 2018;142:83-87.

16. Johnson WL. Is metallic glass poised to come of age? *Nature Materials*. 2015;14:553-555.

17. Schuh CA, Hufnagel TC, Ramamurty U. Mechanical bahavior of amorphous alloys. *Acta Materialia*. 2007;55(12):4067-4109.

18. Cui C, Ye F, Song G. Laser surface remelting of Fe-based alloy coatings deposited by HVOF. *Surface and Coatings Technology*. 2012;206(8-9):2388-2395.

19. Wu C, Ma M, Liu W, Zhong M, Zhang W, Zhang H. Laser producing Fe-based composite coatings reinforced by in situ synthesized multiple carbide particles. *Materials Letters*. 2008;62(17-18):3077-3080.

20. Zhang P, Yan H, Yao C, Li Z, Yu Z, Xu P. Synthesis of Fe-Ni-B-Si-Nb amorphous and crystalline composite coatings by laser cladding and remelting. *Surface and Coatings Technology*. 2011;206(6):1229-1236.

21. May JE, de Oliveira MF, Afonso, CRM, Sá Lisboa RD, Kuri SE. Amorphous phase partitioning in FeCo-based metallic glass alloys. *Journal of Non-Crystalline Solids*. 2004;348:250-257.

22. Afonso CRM, Bolfarini C, Botta Filho WJ, Kiminami CS. Spray forming of the glass former $Fe_{83}Zr_{3.5}Nb_{3.5}B_9Cu_1$ alloy. *Materials Science and Engineering: A*. 2004;375-377:571-576.

23. Afonso CRM, Bolfarini C, Botta Filho WJ, Kiminami CS. Spray forming of glass former $Fe_{63}Nb_{10}Al_4Si_3B_{20}$ alloy. *Materials Science and Engineering: A*. 2007;449-451:884-889.

24. Rios CT, Afonso CRM, Bolfarini C, Botta Filho WJ, Kiminami CS. Characterization of glass former alloy $Fe_{43.2}Co_{28.8}B_{19.2}Si_{4.8}Nb_4$ processed by spray forming and wedge mold casting techniques. *Materials Science Forum*. 2011;691:23-26.

25. Kim JT, Hong SH, Park HJ, Kim YS, Park GH, Park JY, Lee N, et al. Improving the plasticity and strength of Fe-Nb-B ultrafine eutetic composite. *Materials & Design*. 2015;76:190-195.

26. Jendrzejewski R, Kreja I, Śliwiński G. Temperature distribution in laser-clad multi-layers. *Materials Science and Engineering: A*. 2004;379(1-2):313-320.